

Supplementary information

Facilely Synthesized Crosslinked Gel Polymer Electrolytes for High-Performance Quasi Solid-State Rechargeable Magnesium Batteries

Yukun Sun*, Qinnan Zhou*, Kaiwen Zheng, Feng Xiong, Yan Chen, Eslam Sheha, Jun Yang,

Jiulin Wang, Yanna NuLi†

Experimental Procedure

1. The details of experimental section

1.1 Synthesis of $\text{Mg}(\text{BH}_4)_2$

Magnesium borohydride ($\text{Mg}(\text{BH}_4)_2$) was synthesized using a previously established method.^[1] In detail, 40 mmol of sodium borohydride (NaBH_4 , Aladdin, 98%) and 20 mmol of magnesium chloride (MgCl_2 , Aladdin, 99%) were ball-milled under argon at 200 rpm for 16 hours, with a ball-to-material ratio of 20:1. The resulting mixture was then subjected to Soxhlet extraction using diethyl ether (Sinopharm Chemical Reagent Co., Ltd, 99.9%, pre-dehydrated with 4Å molecular sieves for 48 hours). The extracted clear liquid was vacuum-dried at 40°C to remove the diethyl ether, followed by a gradual heating to 150°C. Subsequently, the mixture was dried under vacuum at 150°C for 2 hours to remove any remaining crystalline diethyl ether. The final product, a white powder, was obtained with an approximate yield of 20%. The above procedures were all conducted under argon atmosphere.

1.2 Preparation of MBC-PEG@GF CGPE

All synthetic procedures were carried out in an argon-filled glovebox, maintaining moisture and oxygen levels below 0.01 ppm at room temperature. Magnesium chloride (MgCl_2 , Aladdin, 99.9%) and polyethylene glycol (PEG, Aladdin, 99%) of varying molecular weights were used as received. Tetrahydrofuran (THF, Adamas, 99.9%) was pre-dehydrated with 4Å molecular sieves for 48 hours. The glass fiber (GF, Whatman, GF/A) membranes were dried under vacuum at 100°C for 24 hours and subsequently stored in the argon-filled glovebox.

$\text{Mg}(\text{BH}_4)_2$ and MgCl_2 were mixed in equimolar proportions and dissolved in THF to prepare a $\text{Mg}(\text{BH}_4)_2$ - MgCl_2 /THF solution where the concentration of $\text{Mg}(\text{BH}_4)_2$ was 0.5 M.^[2] The solution was stirred at room temperature for at least 24 hours before use to ensure complete dissolution and homogeneity, yielding a slightly white, cloudy solution. PEG was dissolved in THF to produce the transparent PEG/THF solution. The concentration and molecular weight of PEG varied, with the optimal formulation being PEG4000 at a concentration of 0.2 g·mL⁻¹.

In this work, GF serves as a mechanical support substrate, providing the essential mechanical properties for the MBC-PEG@GF CGPE. Considering the thickness and porosity of the membrane, the GF/A type is chosen as the optimal substrate. The synthesis of MBC-PEG@GF CGPE was achieved through an in-situ cross-linking reaction inside the GF membrane, driven by

Lewis acid-base interactions. In detail, when assembling coin cells, 180 μL 0.5 M $\text{Mg}(\text{BH}_4)_2\text{-MgCl}_2/\text{THF}$ solution and 180 μL 0.2 $\text{g}\cdot\text{mL}^{-1}$ PEG/THF solution were injected in sequence into a piece of GF positioned in a 2032-type coin cell at room temperature. The in-situ cross-linking reaction proceeds spontaneously, resulting in the formation of MBC-PEG@GF CGPE directly between the anode and cathode.

1.3 Preparation of Mo_6S_8 cathodes

The Mo_6S_8 material was synthesized following established protocols.^[3] Initially, MoS_2 , Cu, and Mo powders were ball-milled together in a molar ratio of 2:1:1. The resulting powder mixture was then blended with iodine and subjected to calcination under an argon atmosphere at 800°C for 24 hours to produce $\text{Cu}_2\text{Mo}_6\text{S}_8$. This intermediate product was subsequently treated in 6 M HCl solution with O_2 bubbling for 12 hours, yielding Mo_6S_8 powder, which was dried under vacuum at 80°C for 24 hours.

To fabricate the Mo_6S_8 cathodes, a slurry comprising Mo_6S_8 , Super P, and PVDF in a mass ratio of 8:1:1 was cast onto stainless steel (SS) foil (10 μm thick). The foil was then cut into circular cathodes with a diameter of 10 mm. The total mass loading of Mo_6S_8 was approximately 1.5 $\text{mg}\cdot\text{cm}^{-2}$. The cathodes were dried under vacuum at 60°C for 24 hours prior to use.

2. The details of characterization section

2.1 Phase/morphology analysis

Raman spectra were acquired in the range of 4000 to 50 cm^{-1} using a Raman spectroscope (Thermo Scientific, USA). Samples were encapsulated in capillaries and stored in an argon environment prior to analysis. Fourier transform infrared (FTIR) spectra were recorded over the range of 4000 to 400 cm^{-1} on a Fourier transform infrared spectroscope (PerkinElmer, Spectrum 100) with a resolution of 4 cm^{-1} and a total of 64 scans.

X-ray diffractometer (XRD, D/MAX-2200/PC, Cu $K\alpha$ radiation) and X-ray photoelectron spectroscope (XPS, Kratos Axis DLD spectrometer with monochromatic Al $K\alpha$ radiation, $h\nu=1486.6$ eV) were utilized for interface analysis. Field Emission Scanning Electron Microscope (FE-SEM, Thermo Fisher Scientific, Apreo 2S) equipped with an energy dispersive X-ray spectrometer (EDS, Thermo Fisher Scientific, 10 KV) was used to identify the morphology of membranes and electrodes.

Solid-state nuclear magnetic resonance spectroscope (Bruker Avance NEO 600 MHz) was

employed to analyze the ^{11}B NMR spectra. The ^{11}B chemical shifts were referenced to boric acid (H_3BO_3) as a solid external standard.

2.2 Mechanical and thermal property analysis

Storage modulus and loss modulus of the polymer electrolytes were measured by a dynamic mechanical analyzer (DMA, TA Instruments, Discovery DMA 850) at 25°C .

Thermogravimetric analysis (TGA) was conducted using a thermal analyzer (TA Instruments, Discovery TGA550) within a temperature range spanning from 50 to 800°C . The heating rate was set at $10^\circ\text{C}\cdot\text{min}^{-1}$, and the entire testing procedure was conducted under nitrogen atmosphere to prevent oxidative degradation. Differential scanning calorimetry (DSC) was employed to determine the glass transition temperature of the CGPE on a differential scanning calorimeter (PerkinElmer, DSC 8000). Samples were analyzed under nitrogen atmosphere, with the heating and cooling rates set at $5^\circ\text{C}\cdot\text{min}^{-1}$.

Gel permeation chromatography (GPC) analyses were conducted using a HLC-8320GPC (Japan). The eluent used was THF (HPLC grade), with a flow rate of $1\text{ mL}\cdot\text{min}^{-1}$ and a temperature of 30°C .

2.3 Electrochemical property analysis

All testing coin cells were assembled in an argon-filled glovebox, maintaining moisture and oxygen concentrations below 0.01 ppm , using a CR2032-type coin cell configuration.

Cyclic voltammetry (CV) was performed in CR2032-type coin cells, employing stainless steel (SS) foil as the working electrode and magnesium as the counter electrode, using an electrochemical workstation (Solartron Analytical). The scan rate was controlled at $5\text{ mV}\cdot\text{s}^{-1}$.

Electrochemical impedance spectroscopy (EIS) measurements were carried out with the same electrochemical workstation over a frequency range from 10^6 Hz to 0.01 Hz .

The ionic conductivity of polymer electrolytes was evaluated using two stainless steel (SS) slices (16 mm in diameter) that sandwiched the polymer electrolyte within CR2032-type coin cells. The ionic conductivity was calculated using the following equation:

$$\sigma = \frac{d}{R \cdot S}$$

where R represents the resistance according to EIS measurement, d represents the thickness of the membrane, and S is the area of the contact between the SS and the gel polymer electrolyte.

The electronic conductivity of polymer electrolytes was assessed using two stainless steel (SS) slices (16 mm in diameter) that sandwiched the polymer electrolyte within CR2032-type coin cells. A static polarization potential of 5 mV was applied to measure the current response. The electronic conductivity was then calculated using the same equation employed for determining the ionic conductivity.

The Mg^{2+} transference number was assessed in $\text{Mg}||\text{Mg}$ symmetric cells through EIS measurements conducted both before and after the chronoamperometry (CA) test. Subsequently, it was calculated utilizing the Bruce–Vincent–Evans equation:

$$t_{\text{Mg}^{2+}} = \frac{I_s}{I_0} \cdot \frac{V - I_0 \cdot R_0}{V - I_s \cdot R_s}$$

where V represents the voltage polarization applied; I_s and R_s denote the steady-state current and resistance, respectively; I_0 and R_0 represent the initial current and resistance. In this study, a voltage polarization of 20 mV was applied.

Galvanostatic charge-discharge tests were performed on $\text{SS}||\text{Mg}$ asymmetric cells, $\text{Mg}||\text{Mg}$ symmetric cells, and $\text{Mo}_6\text{S}_8||\text{Mg}$ full cells using the LAND battery test system (LAND CT2001A). Specifically, the $\text{Mo}_6\text{S}_8||\text{Mg}$ full cells were assessed over a voltage range of 0.1 to 1.65 V at room temperature and 0.1 to 1.5 V at 50°C. High-rate tests were conducted following an initial 5 cycles activation at 0.2 C. All cells were tested after standing under 30°C for at least 12 hours.

The $\text{Mo}_6\text{S}_8||\text{Mg}$ pouch cells were assembled with larger sized Mo_6S_8 cathode (5.8 cm×4.5 cm), MBC-PEG@GF CGPE (8 cm×6 cm) and Mg anode (5.8 cm×4.5 cm) in an argon-filled glovebox environment where the concentration of O_2 and H_2O was controlled under 0.01 ppm. The pouch cells were sealed under quasi vacuum (about 0.01 MPa) and were tested after standing under 30°C for at least 24 hours.

3. The details of theoretical calculation section

3.1 Density functional theory (DFT) theoretical calculation

All molecular structures were meticulously optimized using the Lee-Yang-Parr gradient-corrected correlation functional (B3LYP) method and the 6-311G++(d,p) basis set, employing the SMD solvation model within the Gaussian 16 software package. During optimization, all atoms underwent complete relaxation. Calculations were performed under standard conditions of 298 K and 1 atm pressure, ensuring that all computed results confirmed the

absence of imaginary frequencies. Visualization of theoretical calculations was conducted using GaussView 6.1.1.

3.2 Molecular dynamics (MD) theoretical calculation

All-atom molecular dynamics (MD) simulations of $\text{Mg}(\text{BH}_4)_2\text{-MgCl}_2/\text{THF}$ solution, MBC-PEG GPE, and MBC-PTHF GPE were conducted using GROMACS 2024.2. The systems were built by inserting an appropriate ratio of ions and molecules into cubic boxes according to the experimental formula. Force field parameters were assigned using the OPLS-AA force field, and the OPLS-AA parameters with 1.14*CMIA partial atomic charges for Mg^{2+} , Cl^- , BH_4^- ions, PEG, and PTHF molecules were generated using LigParGen.^[4]

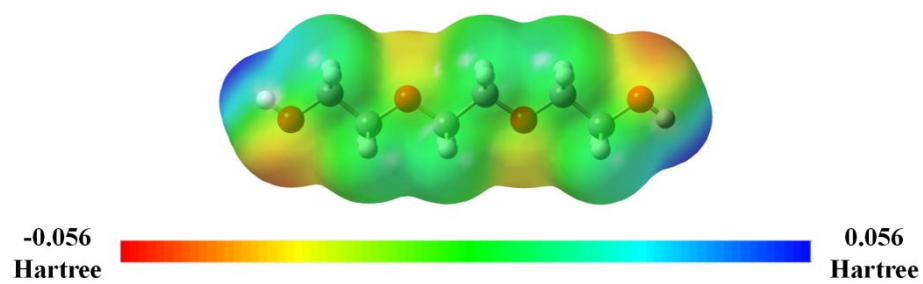
To streamline the simulations, interactions between BH_4^- ions and terminal -OH groups of PEG and PTHF were neglected. To obtain the electrolyte structure, initial simulations were run in the isothermal-isobaric (NPT) ensemble at 298 K for 1 ns to ensure equilibrium salt dissociation. Subsequently, 5 ns canonical (NVT) ensemble simulations were conducted, and the final 1 ns trajectory was analyzed to characterize the electrolyte structure.^[5]

Simulations of Mg^{2+} transport under applied electric field utilized potentials ranging from 1 to 5 $\text{V}\cdot\text{nm}^{-1}$ along the z-axis.^[6]

Each simulation employed a time step of 1 fs. Visualization of simulation results was performed using VMD 1.0.0.1.

4. Supplementary figures

(a)



(b)

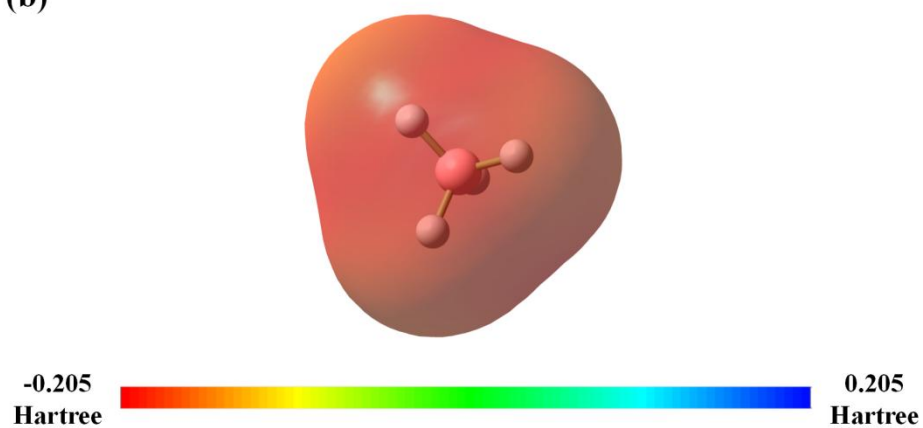


Figure S1. Calculated electrostatic potential (ESP) of (a) PEG short chain and (b) BH_4^- anion.

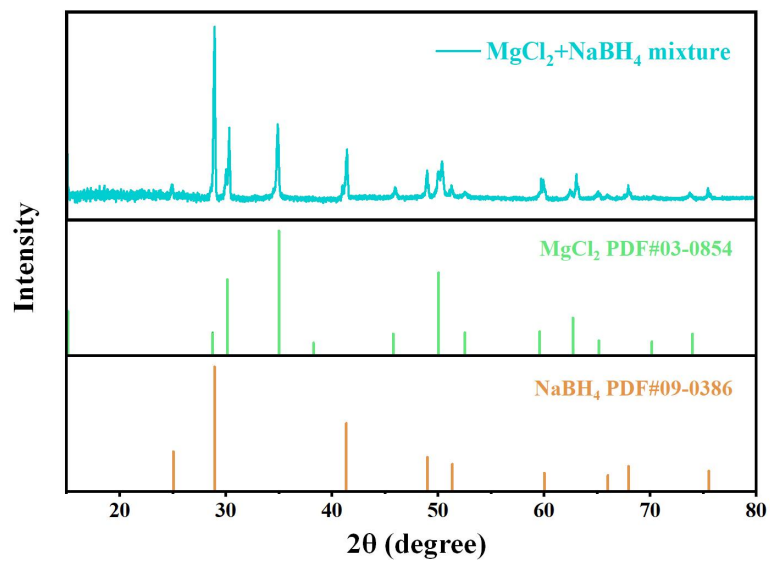


Figure S2. XRD analysis of raw materials containing MgCl₂ and NaBH₄.

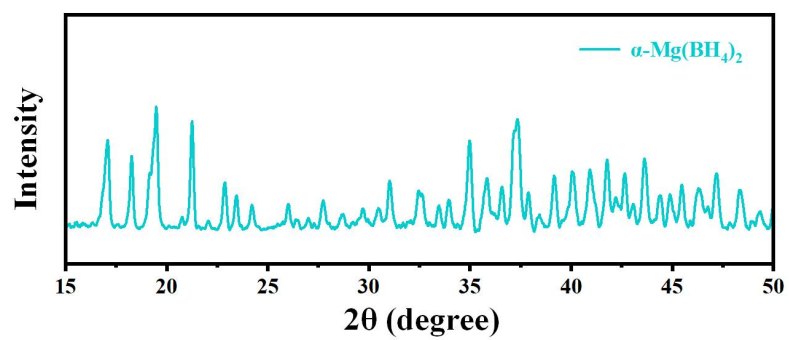


Figure S3. XRD analysis of the synthesized $\text{Mg}(\text{BH}_4)_2$. The peak results are in accordance with results from previous work.^[1]

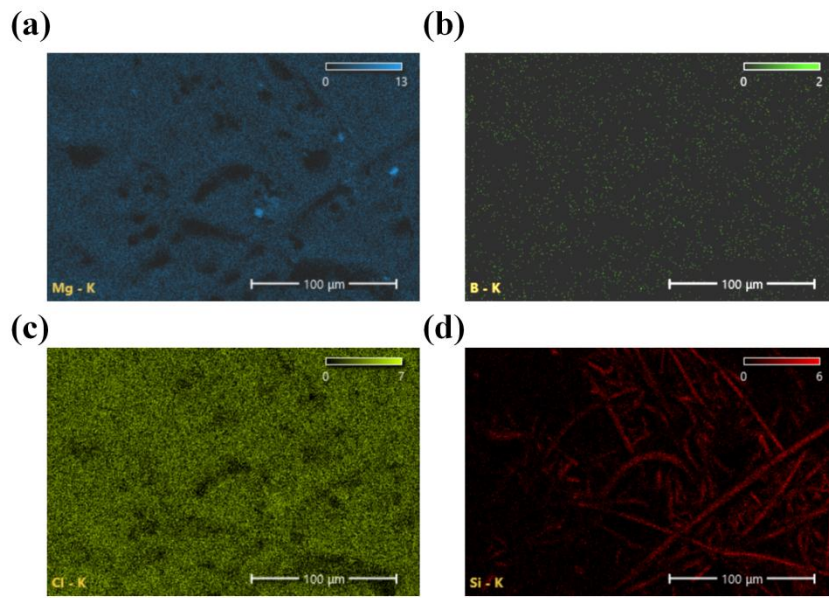


Figure S4. The corresponding EDX elemental maps of a) Mg, b) B, c) Cl and d) Si of Figure 2c.

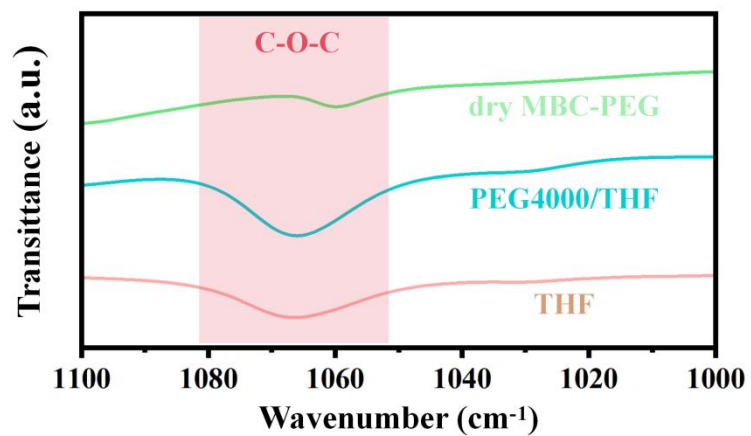


Figure S5. The specific region of FTIR spectra of dry MBC-PEG GPE, PEG4000/THF solution and pure THF. The region is corresponding to the stretching vibration of C-O-C structure.

(a)



(b)



Figure S6. Thickness tests of MBC-PEG@GF CGPE and MBC-PTHF@GF CGPE.

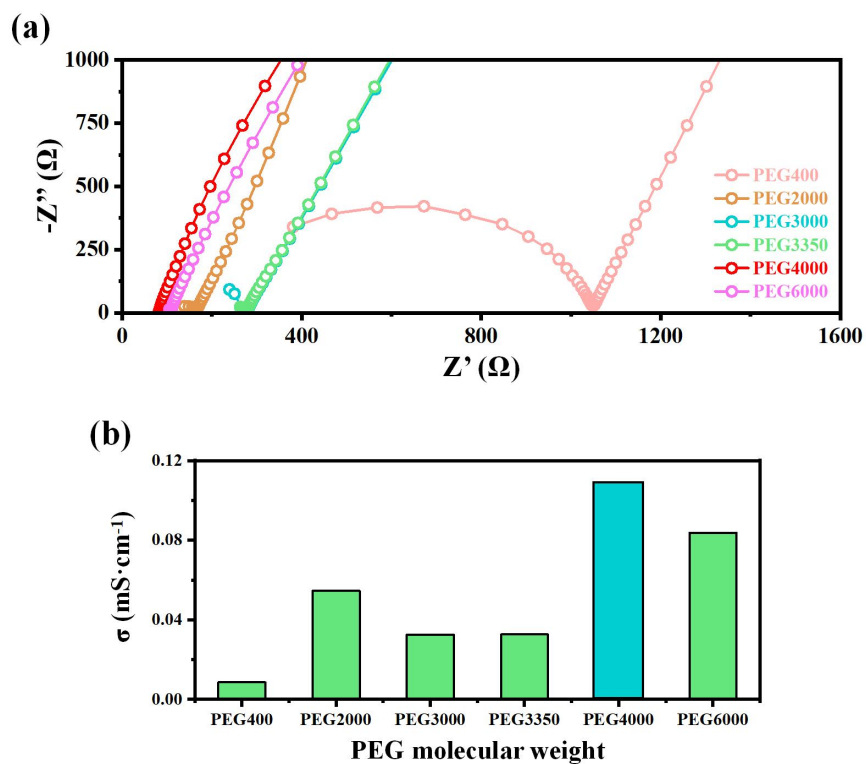


Figure S7. (a) Ionic conductivity of MBC-PEG@GF CGPE synthesized from PEG with different molecular weights at 30°C. (b) The comparison of ionic conductivity of MBC-PEG@GF CGPE synthesized from PEG with different molecular weights at 30°C.

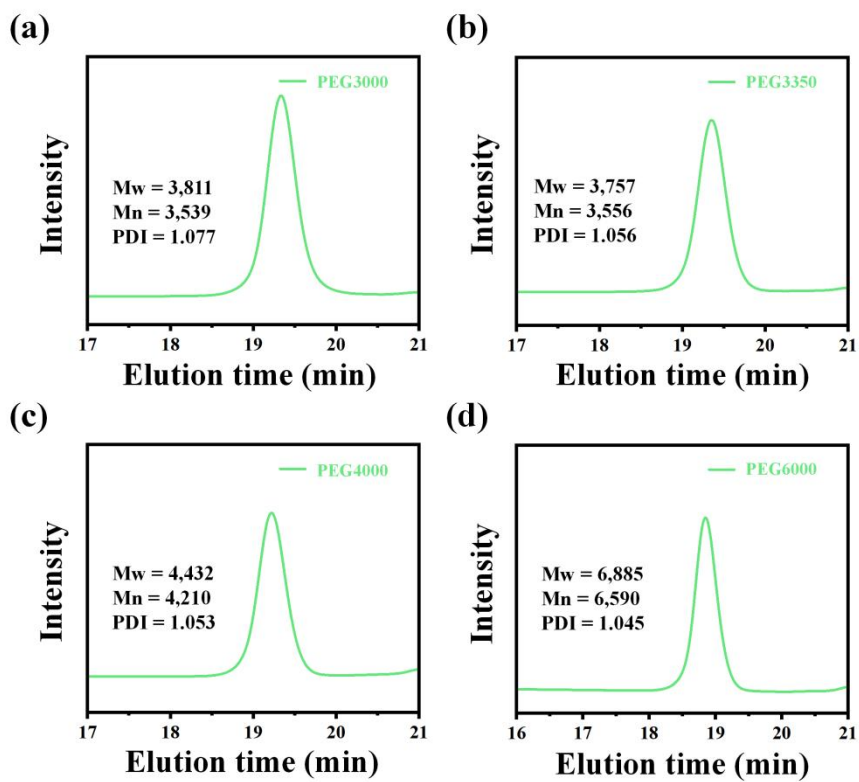


Figure S8. GPC analysis of (a) PEG3000, (b) PEG3350, (c) PEG4000 and (d) PEG6000.

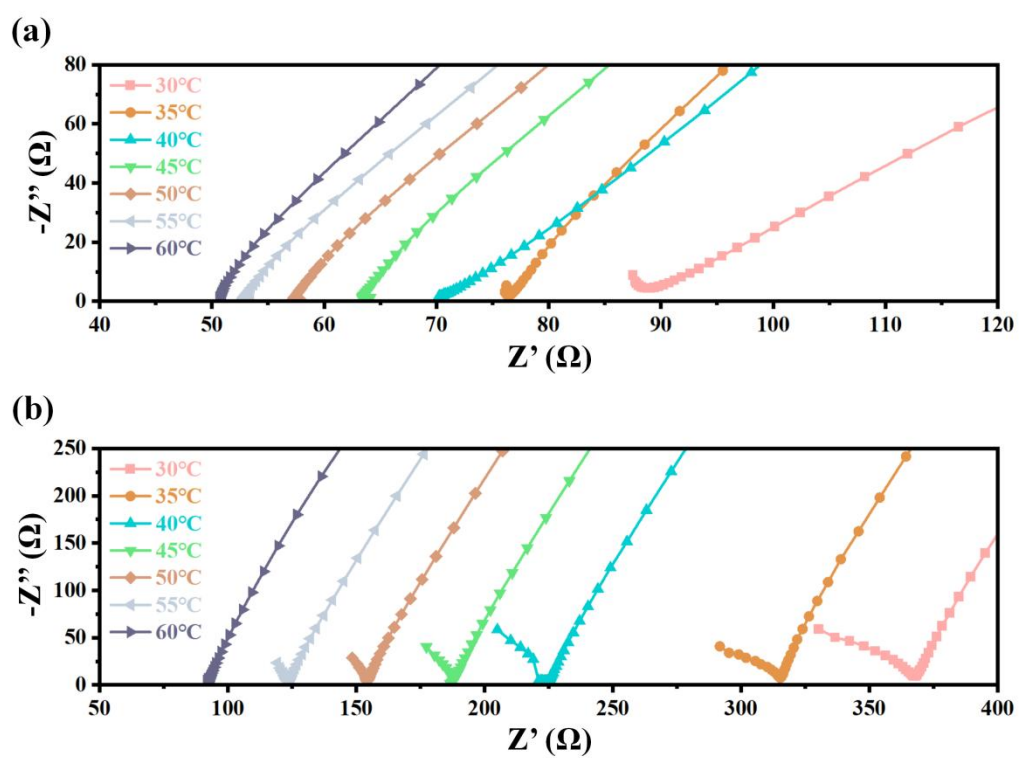


Figure S9. (a) Impedance spectra of SS||MBC-PEG@GF||SS cell at different temperatures. (b) Impedance spectra of SS||MBC-PTHF@GF||SS cell at different temperatures.

Table S1. Specific parameters of the $t_{Mg^{2+}}$ tests exhibited in **Figure 3b**.

Relevant parameters	Test values
MBC-PEG@GF CGPE	
I_0	0.426 μA
I_s	0.183 μA
R_0	175591.8 Ω
R_s	283718.5 Ω
ΔV	0.02 V
$t_{Mg^{2+}}$	0.74

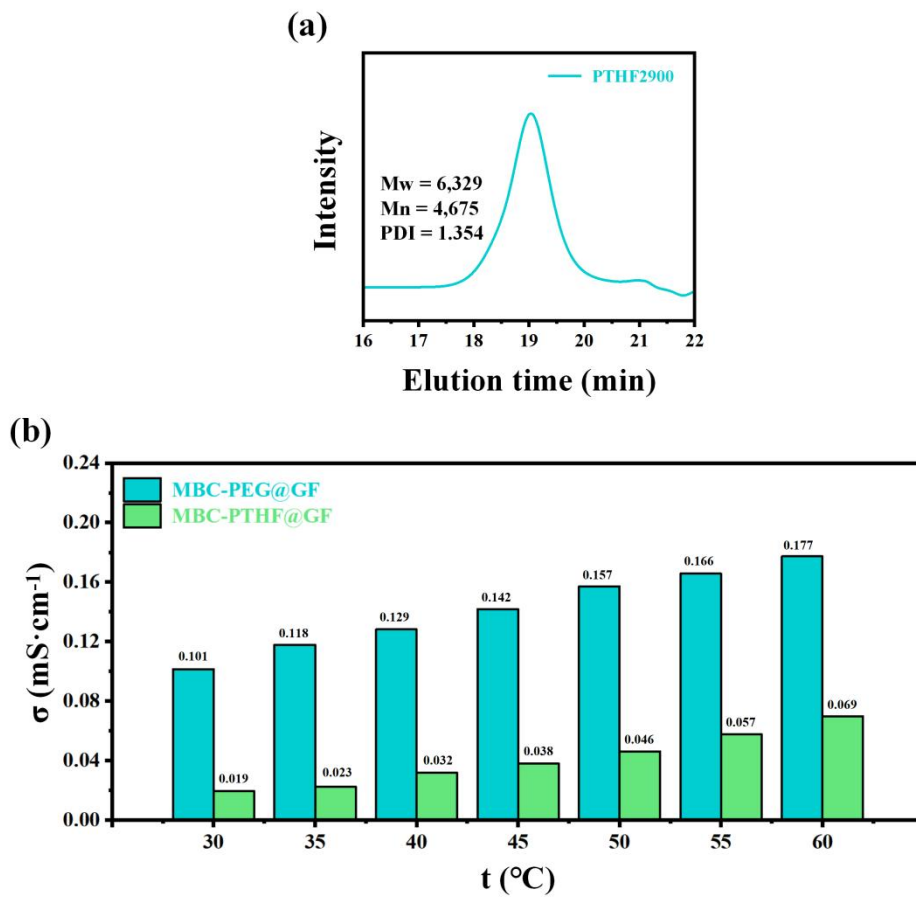


Figure S10. (a) GPC analysis of PTHF. (b) Comparison of ionic conductivity of MBC-PEG@GF CGPE and MBC-PTHF@GF CGPE at different temperatures.

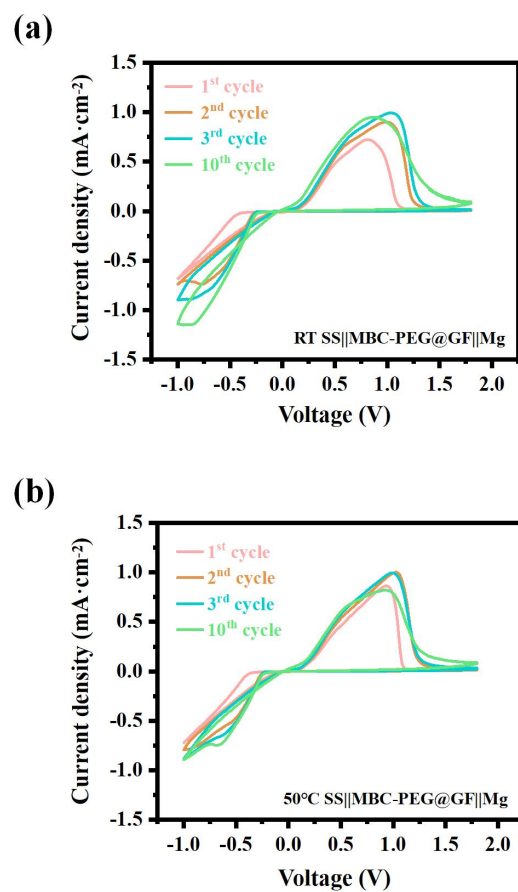


Figure S11. CV curves of SS||MBC-PEG@GF||Mg asymmetric cells at (a) room temperature and (b) 50°C.

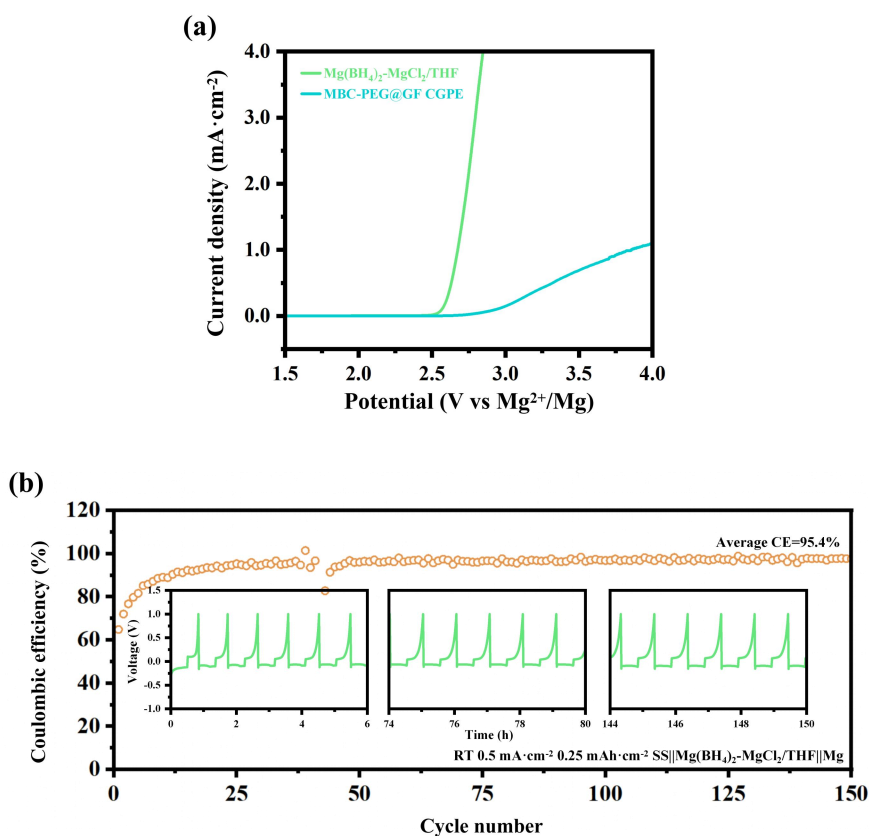


Figure S12. (a) The LSV profiles of the Mg(BH₄)₂-MgCl₂/THF liquid electrolyte and MBC-PEG@GF CGPE at a scan rate of 1 mV·s⁻¹ on the SS current collector under room temperature. (b) Coulombic efficiency of the SS||Mg(BH₄)₂-MgCl₂/THF||Mg cell cycled at a discharge-charge current density of 0.5 mA·cm⁻² and an areal capacity of 0.25 mAh·cm⁻². The inset exhibits the corresponding voltage-time profiles at different stages with a charging cut-off voltage of 1.0 V.

LSV tests were performed using SS current collectors to assess the oxidative stability of both the Mg(BH₄)₂-MgCl₂/THF liquid electrolyte and the MBC-PEG@GF CGPE. As shown in **Figure S12a**, the addition of the PEG polymer matrix significantly widens the electrochemical oxidation window, indicating enhanced oxidative stability. This improvement can be attributed to the decrease of easily oxidizable B-H groups in the MBC-PEG@GF CGPE, which are consumed by the terminal -OH groups on the PEG polymer matrix. Besides, according to **Figure S12b**, the reversibility of the Mg plating/stripping process was evaluated using SS current collectors. Compared to the MBC-PEG@GF CGPE (**Figure 4a**), the SS||Mg asymmetric cell with the Mg(BH₄)₂-MgCl₂/THF liquid electrolyte exhibited significantly reduced reversibility. The average

Coulombic efficiency of the liquid electrolyte-based cell reached only 95.4% over the first 150 cycles, accompanied by a prolonged activation process and a low initial Coulombic efficiency of 62.7%. These results demonstrate that the MBC-PEG@GF CGPE enhances compatibility with the Mg anode compared to the liquid electrolyte.

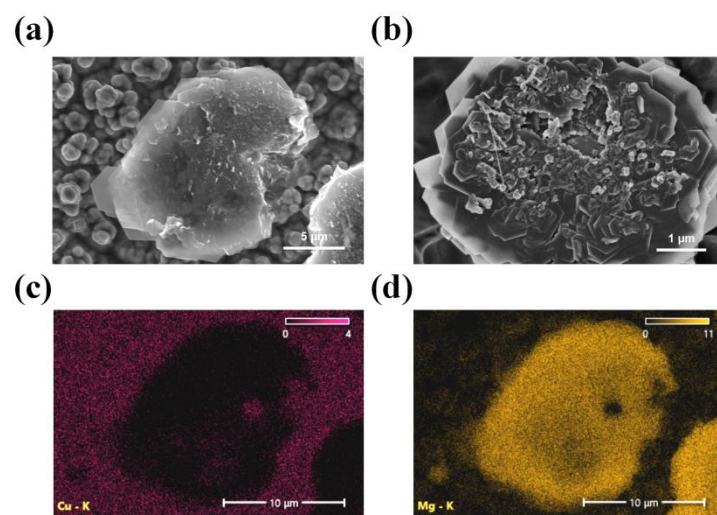


Figure S13. (a) Representative surface SEM image of the Mg deposits on Cu substrate and (b) a higher resolution image. (c-d) The corresponding EDX elemental maps of (c) Cu and (d) Mg.

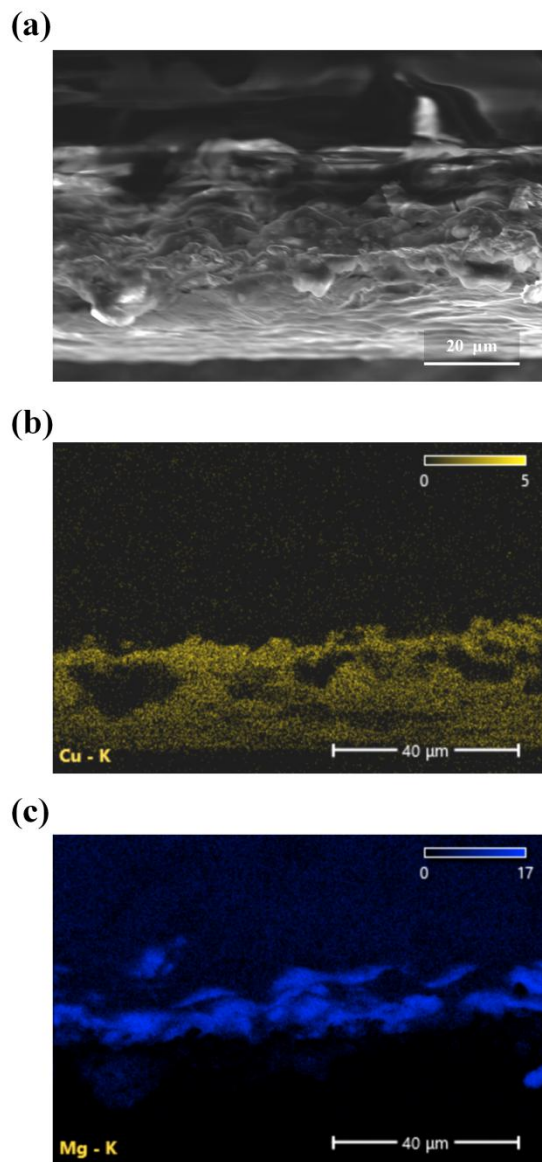


Figure S14. (a) Representative cross-section SEM image of the Mg deposits on Cu substrate. (b-c) The corresponding EDX elemental maps of (b) Cu and (c) Mg.

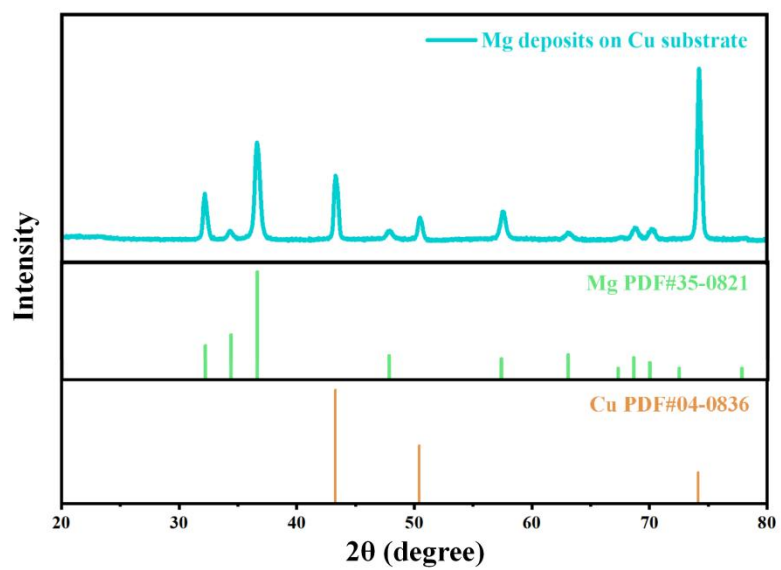
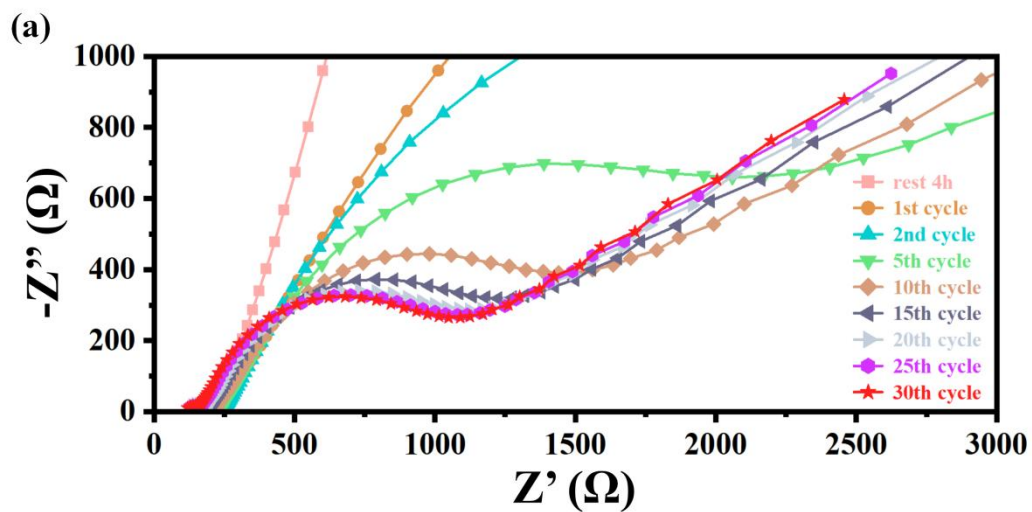
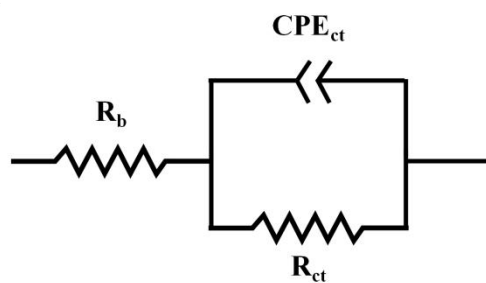


Figure S15. XRD analysis of Mg deposits on Cu substrate.



(b)



(c)

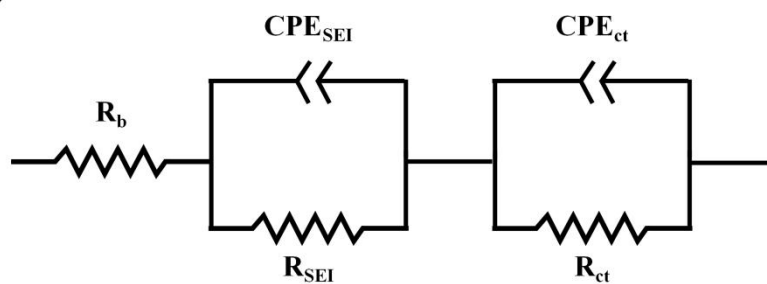
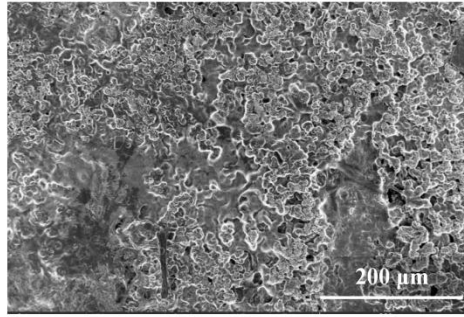


Figure S16. (a) EIS spectra of Mg||MBC-PEG@GF||Mg symmetric cell at different cycling stages. Equivalent circuit model of Mg||MBC-PEG@GF||Mg symmetric cell during (b) resting stage, and (c) cycling stage.

Table S2. Fitting value of R_b , R_{SEI} and R_{ct} of Mg||MBC-PEG@GF||Mg symmetric cell at different cycling stages.

Fitted parameters	rest 4h	After 1st cycle	After 2nd cycle	After 5th cycle	After 10th cycle	After 15th cycle	After 20th cycle	After 25th cycle	After 30th cycle
R_b (Ω)	237.2	237.5	237.8	238.5	215.6	189.4	172.6	159.1	147.9
R_{ct} (Ω)	171610	9513	4853	2667	1695	1063	1225	1167	1133
R_{SEI} (Ω)	—	—	—	—	—	43.4	440.5	384.7	395.3

(a)



(b)

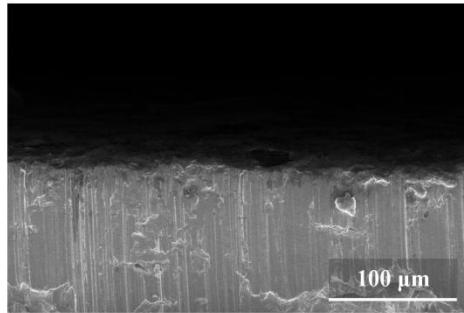


Figure S17. Representative SEM images of (a) surface and (b) cross section of Mg electrode after 200 cycles in Mg||MBC-PEG@GF||Mg symmetric cell at a current density of $0.1 \text{ mA} \cdot \text{cm}^{-2}$.

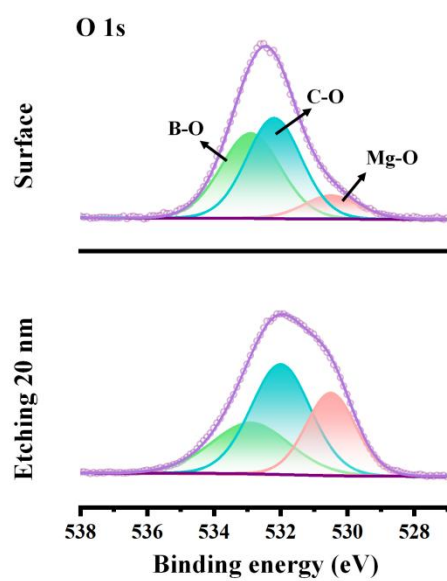


Figure S18. XPS analysis for O 1s of the Mg electrode after 200 cycles in symmetric Mg||MBC-PEG@GF||Mg cell at a current density of $0.1 \text{ mA}\cdot\text{cm}^{-2}$.

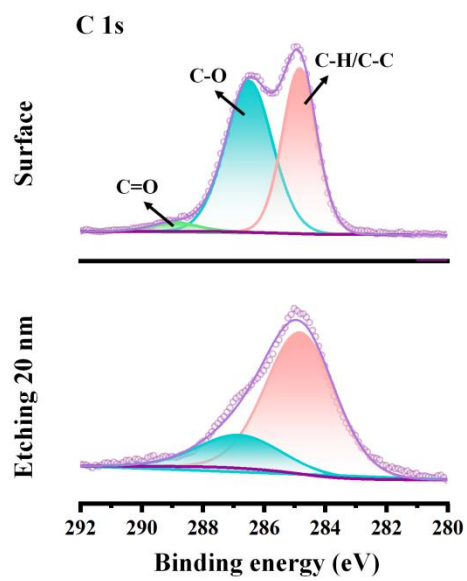


Figure S19. XPS analysis for C 1s of the Mg electrode after 200 cycles in symmetric Mg||MBC-PEG@GF||Mg cell at a current density of $0.1 \text{ mA}\cdot\text{cm}^{-2}$.

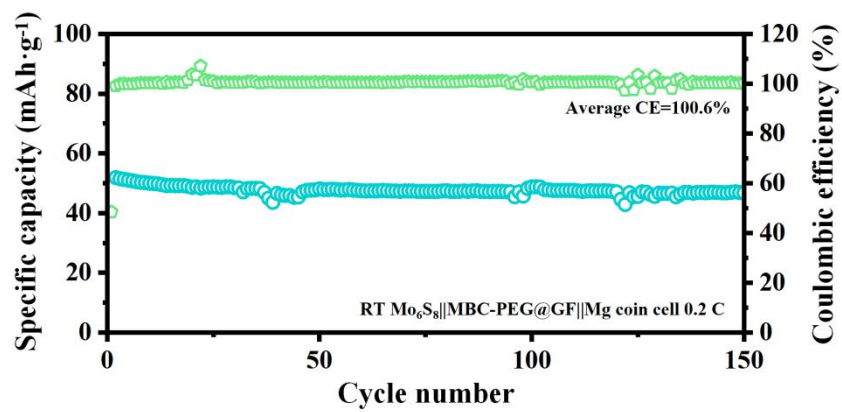


Figure S20. Cycling stability and corresponding CE of $\text{Mo}_6\text{S}_8||\text{MBC-PEG@GF}||\text{Mg}$ coin cell at room temperature, operated at a rate of 0.2 C.

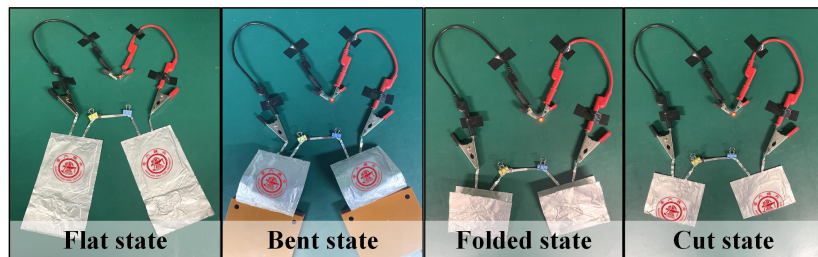


Figure S21. Schematic diagrams of the LED light lightened by $\text{Mo}_6\text{S}_8\|\text{MBC-PEG@GF}\|\text{Mg}$ pouch cells under different states.

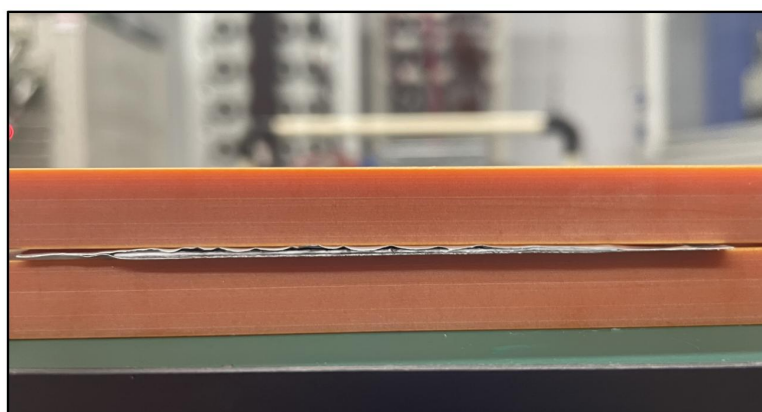


Figure S22. Digital photograph of the cross-section of the cut $\text{Mo}_6\text{S}_8||\text{MBC-PEG@GF}||\text{Mg}$ pouch cell in the pressed condition.

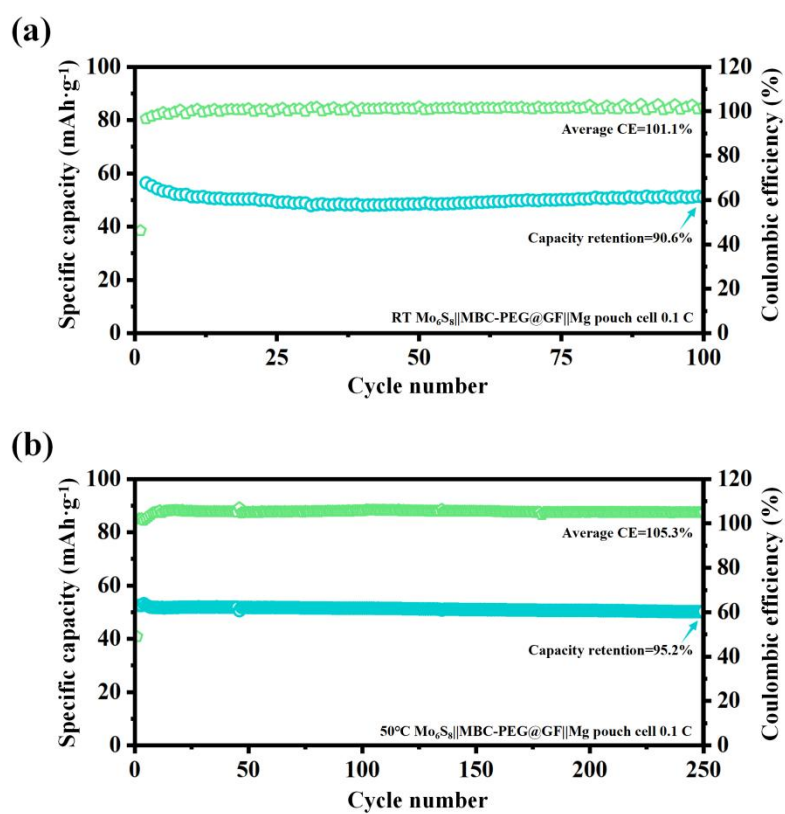


Figure S23. Cycling stability and corresponding CE of $\text{Mo}_6\text{S}_8||\text{MBC-PEG@GF}||\text{Mg}$ pouch cells at (a) room temperature and (b) 50°C, operated at a rate of 0.1 C.

Table S3. Comparison of the Mo₆S₈||MBC-PEG@GF||Mg pouch cell with representative previous works.

Pouch cells	Operating temperature (°C)	Rate	Specific capacity (mAh·g ⁻¹)	Cycles	Reference work
Ketjen black/S MgBOR-PTHF-GPE Mg	RT	0.05 C	~100	15	7 ^[7]
Mo ₆ S ₈ PECH-OMgCl@G3 SSPE Mg	30	0.3 C	~65	100	8 ^[8]
14PAQ@KB 0.5M Mg[B(HFIP) ₄] ₂ /G4 Mg	RT	0.1 C	~130	20	9 ^[9]
LiFePO ₄ APC+LiCl/THF Mg	RT	1 C	103.4	200	10 ^[10]
Mo ₆ S ₈ APC/THF PA-Al@Mg	RT	1 C	20	700	11 ^[11]
S/C 0.3M Mg[B(HFIP) ₄] ₂ /DME Mg	RT	0.05 C	103	100	12 ^[12]
Mo₆S₈ MBC-PEG@GF Mg	RT	0.1 C	51.0	100	This work
	50	0.1 C	51.4	250	
	RT	0.5 C	45.1	1000	
	50	0.5 C	30.9	300	

Reference

- [1] K. Chłopek, C. Frommen, A. Léon, O. Zabara, M. Fichtner, *Journal of Materials Chemistry* **2007**, *17*, 3496-3503.
- [2] A. Du, H. Zhang, Z. Zhang, J. Zhao, Z. Cui, Y. Zhao, S. Dong, L. Wang, X. Zhou, G. Cui, *Advanced Materials* **2019**, *31*, 1805930.
- [3] M. Mao, Z. Lin, Y. Tong, J. Yue, C. Zhao, J. Lu, Q. Zhang, L. Gu, L. Suo, Y.-S. Hu, *ACS nano* **2019**, *14*, 1102-1110.
- [4] L. S. Dodda, J. Z. Vilseck, J. Tirado-Rives, W. L. Jorgensen, *The Journal of Physical Chemistry B* **2017**, *121*, 3864-3870.
- [5] W. Zhao, Z. Pan, Y. Zhang, Y. Liu, H. Dou, Y. Shi, Z. Zuo, B. Zhang, J. Chen, X. Zhao, *Angewandte Chemie International Edition* **2022**, *61*, e202205187.
- [6] Z. Yu, D. G. Mackanic, W. Michaels, M. Lee, A. Pei, D. Feng, Q. Zhang, Y. Tsao, C. V. Amanchukwu, X. Yan, *Joule* **2019**, *3*, 2761-2776.
- [7] L. Wang, Z. Li, Z. Meng, Y. Xiu, B. Dasari, Z. Zhao-Karger, M. Fichtner, *Energy Storage Materials* **2022**, *48*, 155-163.
- [8] X. Ge, F. Song, A. Du, Y. Zhang, B. Xie, L. Huang, J. Zhao, S. Dong, X. Zhou, G. Cui, *Advanced Energy Materials* **2022**, *12*, 2201464.
- [9] Y. Xiu, Z. Li, V. Bhaghavathi Parambath, Z. Ding, L. Wang, A. Reupert, M. Fichtner, Z. Zhao-Karger, *Batteries & Supercaps* **2021**, *4*, 1850-1857.
- [10] Z. Zhang, H. Xu, Z. Cui, P. Hu, J. Chai, H. Du, J. He, J. Zhang, X. Zhou, P. Han, *Journal of Materials Chemistry A* **2016**, *4*, 2277-2285.
- [11] T. Wen, S. Tan, R. Li, X. Huang, H. Xiao, X. Teng, H. Jia, F. Xiong, G. Huang, B. Qu.
- [12] L. Wang, P. Jankowski, C. Njel, W. Bauer, Z. Li, Z. Meng, B. Dasari, T. Vegge, J. M. G. Lastra, Z. Zhao-Karger, *Advanced Science* **2022**, *9*, 2104605.